ACS APPLIED MATERIALS & INTERFACES

www.acsami.org

Research Article

Nanofiber-Based Substrate for a Triboelectric Nanogenerator: High-Performance Flexible Energy Fiber Mats

Sk Shamim Hasan Abir, Muhtasim Ul Karim Sadaf, Sunanda Kumar Saha, Ahmed Touhami, Karen Lozano,* and Mohammed Jasim Uddin*

Cite This: *ACS Appl. Mater. Interfaces* 2021, 13, 60401−60412

Read Online

ACCESS | Metrics & More | Article Recommendations | Supporting Information

ABSTRACT: Flexible and stretchable triboelectric nanogenerators (TENGs) are the next-generation systems for wearable and portable electronics. In this study, we have demonstrated an all nanofiber-based TENG for energy harvesting and biomechanical sensing applications. The TENG was prepared using the Forcespinning (FS) method to produce poly(vinylidene fluoride) (PVDF) and thermoplastic polyurethane (TPU) nanofiber (NF) membranes. The TPU nanofiber membranes were interfaced with a homogeneously sputtered gold nanofilm. The experimental characterization of the PVDF-TPU/Au NF-TENG revealed that surface interfaced with dispersed gold in a TPU fiber membrane produced a maximum open-circuit voltage of 254 V and a short-circuit current of 86 μA output at a 240 bpm load frequency, which was, respectively, 112 and 87% greater than bare PVDF-TPU NF-based TENG. All systems were composed of an active contact surface area of 3.2 × 2.5 cm^2. Furthermore, the TENG was able to light up 75 LEDs (1.5 V of each) by the hand-tapping motion. The resistive load and capacitor test results exemplified a TENG offering a simple and high-performance self-chargeable device. Furthermore, we have tested the TENG's response for biomechanical movements at different frequencies, suggesting the TENG's potential to be also used as a cost-effective self-powered flexible body motion sensor.

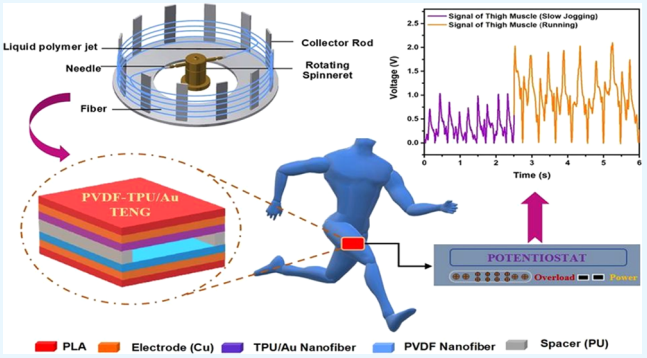

KEYWORDS: *forcespinning, poly(vinylidene fluoride) nanofibers, thermoplastic polyurethane nanofibers, triboelectric nanogenerator, biomotion sensor*

1. INTRODUCTION

Over the last few years, with the expansion of the flexible and stretchable wearable electronic devices, portable power storage for powering small electronics has received an increasing deal of attention by researchers.[1,2] Conventional power sources, like batteries, often face a limited life span, heavy weight, and lack of ecofriendliness.[3,4] To resolve these issues, various modes of nanogenerators have been introduced that can convert solar, thermal, mechanical, and even, chemical energy into continuous and maintenance-free electricity.[5] These nanogenerators typically utilize phenomena such as piezoelectricity, pyroelectricity, photoelectricity, and the electromagnetic effect to harvest energy.[6,7] Developed systems have shown promising potential though still lack a high-power output. Another highly energy-efficient mechanism is the triboelectric effect that can harness electricity from mechanical energy.[8]

The phenomenon of triboelectricity has been known for over 2600 years and it is very common in our day-to-day life. Triboelectricity can be easily explained as the transfer of charges due to the friction between two substances. Yet, the actual mechanism of triboelectricity is still a topic for debate.[9] The knowledge of triboelectricity was not applied much for practical applications until 2012, when Wang et al. first reported on the triboelectric phenomenon used to scavenge ambient mechanical energy and since then a triboelectric nanogenerator (TENG) has been gaining great interest among the researchers due to its potential for light weight, easy fabrication, durability, robustness, and cost effectiveness.[10] Wang et al. also provided a wide list of triboelectric materials and suggested their effective pairing; this came along with some important theoretical suggestions, which has helped in understanding different modes of triboelectric operation.[11] Currently, TENGs are being highly exploited as energy harvesters and self-powered sensors.[12] There are different working modes of TENG like a single-electrode mode, free-standing mode, sliding mode, and contact−separation mode. Among the abovementioned modes, the contact−separation

Received: September 17, 2021
Accepted: November 29, 2021
Published: December 9, 2021

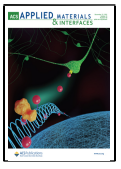

https://doi.org/10.1021/acsami.1c17964
ACS Appl. Mater. Interfaces 2021, 13, 60401−60412

mode is the preferred one, given its ease of fabrication and a higher triboelectric yield.[13] The contact−separation mode TENG works based on the principle of the electrification of two layers followed by the triboelectric effect after they get separated from their initial contact mode.[14] Charges are generated while the top and bottom layers are continuously separated and contacted. This causes a potential difference between two layers and results in current flowing back and forth in the external circuit to balance the surface potential through electrodes, which are already connected to the triboelectric layers. The selection of the triboelectric material is critical to develop charge generation and one of the key considerations to fabricate the TENG.[5,10] Polymers have been widely used for making the layered TENG cell, given their flexibility and lack of environmental corrosion.[15] Polymers with functional groups capable of giving off electrons during mechanical bending and stretching are used as a positive layer, while those with functional groups prone to accepting electrons are used as a negatively charged layer.[16]

The performance of the nanogenerator depends on the frictional contact area, surface chemical properties, charge density, and dielectric properties of the TENG materials. Some of the commonly used materials are poly(vinylidene fluoride) (PVDF),[17] poly(tetrafluoroethylene) (PTFE),[18] poly(dimethylsiloxane) (PDMS),[19] polyimide (PI),[8] poly(vinylidene fluoride-trifluoroethylene) (PVDF-TrFE),[20] poly(vinylidene fluoride-*co*-hexafluoropropene) (PVDF-HFP),[21] poly(vinyl chloride) (PVC),[22] poly propylene (PP),[23] and polyacrylonitrile (PAN).[24] These polymeric systems are used in a variety of forms such as thin films, nanofibers, nanocomposites, and aerogels,[18,25] and all as the negative layer owing to high charge affinity, flexibility, high dipole moment, and durability, all of which are important parameters not only for harnessing mechanical energy but also for functioning as UV detectors,[26] antibacterial and air filtration systems,[27,28] and biomechanical motion- and pressure-sensing devices.[29] To harness mechanical energy and capitalize the TENGs in wearable electronics and human motion detection applications, the selection of the positive layer is of utmost importance. Most of the reports have relied on the use of aluminum (Al),[30] copper (Cu),[19] silver (Ag),[31] polymeric materials (e.g., nylon,[16] thermoplastic polyurethane (TPU),[23] cellulose,[32] poly(3-hydroxybutyrate-*co*-3-hydroxyvalerate) (PHBV),[33] and poly(vinyl alcohol) (PVA)[27]) as the preferred materials.

Compared to a polymer film-based triboelectric layer, which favors brittleness resulting in the absence of mechanical robustness, fiber-based TENGs offer more distinctive and inherent advantages like stretchability and most importantly a larger effective contact surface area.[23] In addition, due to great flexibility and breathability, nanofiber-based TENGs can also be used as active sensors to detect the mechanical response of human motion.[34] The main advantage of TENG sensors is that they can perform without an external power supply.[35] Typically, sensors are employed to detect a target signal but this multifunctional TENG can serve both as an energy-harvesting device as well as a self-powered sensor.[36,37] The prime consideration of wearable electronics is to offer stable but repeated signals with the same time interval; nanofiber-based TENG offers string potential.[38] Considering the excellent electrical and structural properties of nanofiber-based TENGs, these can be easily attached to human skin, and moreover, can easily distinguish different bending angles of human body parts according to their posture.[39] Nanofiber-based TENG layers have been developed using the electrospinning technique; nanofiber membranes with nano- to microscale fiber diameters, high surface area, high porosity, and small pore size have been tested.[19,30] Electrospinning, the most common process to synthesize nanofibers, uses electrostatic forces to make fine fibers. However, this procedure has some intrinsic drawbacks, which are mostly related to a low fiber output. As a consequence, in this study, we have used for the first time the Forcespinning (FS) technique, a cost-effective technique with an unparalleled fiber yield. FS uses centrifugal force to prepare nanofibers,[40,41] and its production rate, at the lab scale, is about 1 g/min compared to 0.1 g/h. Commonly experienced in electrospinning, the FS output is 600 times.[42,43]

In this study, we prepared a TENG system composed fully of nanofiber layers, where the prepared PVDF nanofiber membranes were being used as the tribonegative layers. PVDF is an interesting polymer, which possesses the polymorphic nature, α, β, γ, δ, and ε phases; among these, the α phase is nonpolar while the β phase has a strong polar response.[16] The β phase is induced more effectively over other phases when the continuous and homogeneous PVDF NFs were stretched out from polymer solution by centrifugal force,[43] and this yields electroactive characteristics, especially high polarizability and dielectric properties that promote a significant electrical output of the TENGs.[44] Compared to other positive polymers, TPU has been studied very little in the application of nanogenerator fields. TPU has a good charge density difference compared to PVDF;[45] hence, in our experiments, we utilized TPU NFs as the electropositive layer due to its high contact surface structure, mechanical stretchability, and electron actuation capability.[2,23]

Nevertheless, though there has been a noticeable output achieved in the TENG field, the power output is not up to the mark to use it in real-time wearable electronics. So, there is still room to improve their performance. Currently, researchers are trying surface modification to boost up the performance by incorporating various functional groups with different materials such as metal oxides,[24,28] nanoparticles,[1] carbonaceous material (e.g., graphene oxide (GO),[33] multiwall carbon nanotube (MWCNT),[20] silver nanowires (Ag-NW),[27] and MXene materials[16]) within the TENG materials. Even though surface modification of these triboelectric layers has shown to improve dielectric constants and high charge density difference between the two layers, the methods of introducing these additional materials often present difficulties, given a complicated synthesis or challenges to prevent agglomeration or precipitation during the making of a polymer solution to produce fibers.[3] To overcome these drawbacks, deposition of metal by sputtering can be a plausible solution. Sputtering of a novel metal on a polymer matrix to produce a metal−polymer composite and analyzing functional polymer−metal interfaces has indeed significant importance to fabricating organic electronics, organic photovoltaics (OPVs), and sensors.[46−48] Schwartzkopf et al. demonstrated that the Au sputtered on polystyrene (PS) thin films exhibited remarkable changes in structural and optoelectronic properties for different Au regimes as a function of layer thicknesses (nucleation, isolated island growth, growth of larger aggregates via partial coalescence, and continuous layer growth).[49] The optical reflectivity of the pristine gray-blue PS film showed color tunability at the interface from a dark blue color due to isolated nanoclusters to a bright red color due to larger Au aggregates

https://doi.org/10.1021/acsami.1c17964
ACS Appl. Mater. Interfaces 2021, 13, 60401−60412

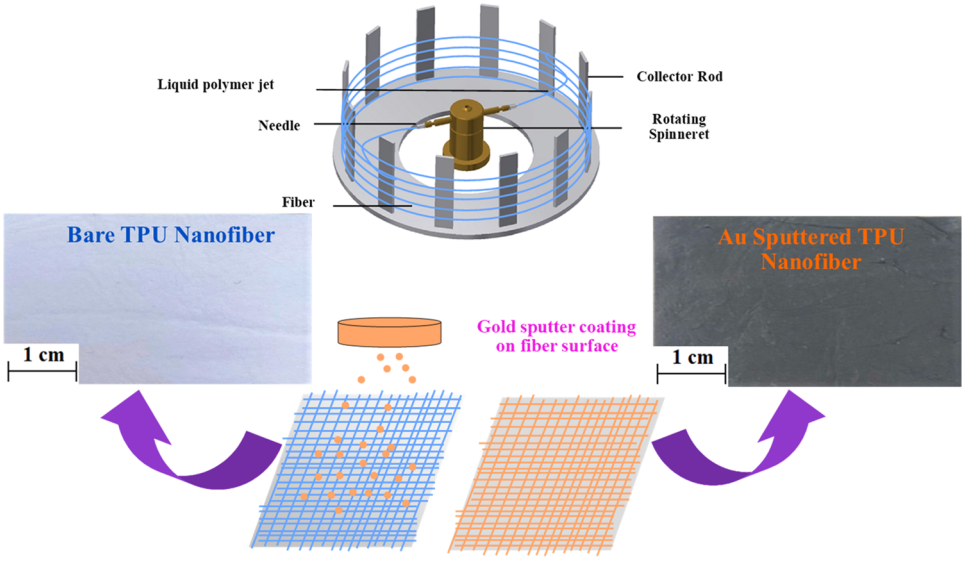

Figure 1. Schematic diagram of fabrication of the nanofiber by the FS technique[40] and gold (Au) sputter coating on the fiber surface.

in the UV/vis regime. Additionally, it was elucidated that near-surface enrichment of Au in a PS matrix can be achieved by sputter deposition, which impacts Au adhesion due to the formation of an embedding Au layer.[50] Moreover, the high-rate deposition of gold resulted in a smoother Au film surface, owing to the smaller particles growing in shorter time intervals resulting from earlier onset of thin film percolation and high density of initial particles due to the nucleation probability increase caused by an enhanced influence of random nucleation.[51] In addition, Roth et al. illustrated that the presence of the imprinted ridges that introduced macroscopically curved structures on the polymer fiber can result in morphological deviation from the mean gold layer morphology.[52]

Here, in our work, we used a simple and straightforward technique, depositing gold (Au) on the surface of the TPU nanofiber membrane using a plasma-assisted sputter coating technique. Owing to the amplified optimal surface roughness and electrochemical properties, gold has been used in TENG and sensory applications.[53,54] Modified Au nanorod and flower-shaped micro-/nanostructures have demonstrated a heightened effective contact surface and TENG output performance.[55,56] Furthermore, using an Au coating added environmental protection.[56] The experimental investigation illustrated that the embedded Au layer on the TPU surface resulted in a high triboelectric open-circuit voltage and short-circuit current output compared to the base PVDF/TPU nanogenerator cell. In addition, the nanofiber-based triboelectric nanogenerator (NF-TENG) showed a strong potential of charging small electronics within a short period of time and a very sensitive and effective biomechanical motion sensor.

2. EXPERIMENTAL SECTION

2.1. Materials. Poly [4,4′-methylenebis (phenyl isocyanate)-alt-1, 4-butanediol/di(propylene glycol)/poly caprolactone], which is a methylene-diisocyanate (MDI) thermoplastic polyester/polyether polyurethane (TPU) was obtained from Sigma-Aldrich. KYNAR 741 poly(vinylidene fluoride) (PVDF) powder was purchased from Arkema Inc. HPLC-grade acetone (C_3H_6O), *N*,*N*-dimethylformamide (DMF, ≥99.7%), and dimethylacetamide (DMA, C_4H_9NO) were all obtained from Fisher Scientific. All of the materials were used without any further treatment.

2.2. Preparation of PVDF and TPU/Au Nanofiber Membranes. To make a PVDF polymer solution, 1.1 g of PVDF powder was dissolved in a mixture of 2.35 g of DMA and 1.96 g of acetone in a 20 mL glass vial. The polymer solution was vortexed for 2 min and then mechanically stirred using a magnetic stirrer at 60 °C in a silica oil bath for 24 h at 800 rpm to ensure complete dissolution. In a similar fashion, to obtain a homogeneous solution of TPU, a 16 wt % solution was prepared with DMF as a solvent; the mixture was magnetically at 1000 rpm for 48 h in a silica oil bath at 105 °C. Then, the mixture was kept in scintillation vials and cooled at room temperature before using to make the fibers. Later, 2 mL of prepared solutions was independently injected into the spinneret equipped with a half inch 30 gauge regular needle to spin the fibers using a Cyclone system (Fiberio Technology Corp.). The deposited fibers on the prolonged collectors were collected as nonwoven membranes and subsequently stored in HDPE bags containing a silica desiccant pouch. To fabricate a TPU/Au nanofiber membrane, gold (Au) was sputtered using a Denton Vacuum Desk II (working gas as air) at a 50 mTorr pressure and a 45 mA current for 120 s to deposit a thin layer (about 25 ± 5 nm) on one surface of a fiber mat. A gold (99%) sputter target was used in the experiment, which was obtained from Denton Vacuum, and had a dimension of a 60.325 mm diameter and a 0.0508 mm thickness. The deposition rate of the target was about 0.23 nm/s at a 50 mTorr pressure and a 45 mA current.

2.3. Fabrication of the TENG. To fabricate the NF-TENG, 4.5 × 2.5 cm^2 fiber mats each having an average thickness of 1.0 ± 0.2 mm was cut and attached to commercially available 0.06 mm thick copper (Cu) tape, which acted as electrodes for both positive and negative layers. The two layers were separated by two PU spacers (average thickness: 2.5 ± 0.1 mm) of 2.50 × 0.65 cm^2 on both ends, resulting in a 3.2 × 2.5 cm^2 active contact area of the NF-TENG. A 5.0 × 5.0 cm^2 layer of 3D-printed PLA having 1.5 ± 0.05 mm thickness was attached on the outer side of both electrodes to impart structural support. All tests were conducted under ambient conditions.

2.4. Characterization. The morphology of the PVDF and TPU nanofibers was characterized with a field-emission scanning electron microscope (FESEM) at an acceleration voltage of 1.0 kV (Sigma VP, Carl Zeiss, Jena, Germany). The Fourier transform infrared spectra of the fiber membrane were obtained using a 133 VERTEX 70v FTIR Spectrometer (Bruker) in the attenuated total reflection (ATR) mode. The transmittance data of the nanofiber samples were recorded from 450 to 4000 cm^{-1} wavenumber. AFM measurements were performed on a Bioscope Catalyst AFM (Bruker) mounted on an inverted optical microscope (Ti, Nikon), which can assist in selecting the interesting area on the sample. Fibers were glued to a small piece (1 cm × 1 cm) of double-sided tape and then imaged immediately.

https://doi.org/10.1021/acsami.1c17964
ACS Appl. Mater. Interfaces 2021, 13, 60401−60412

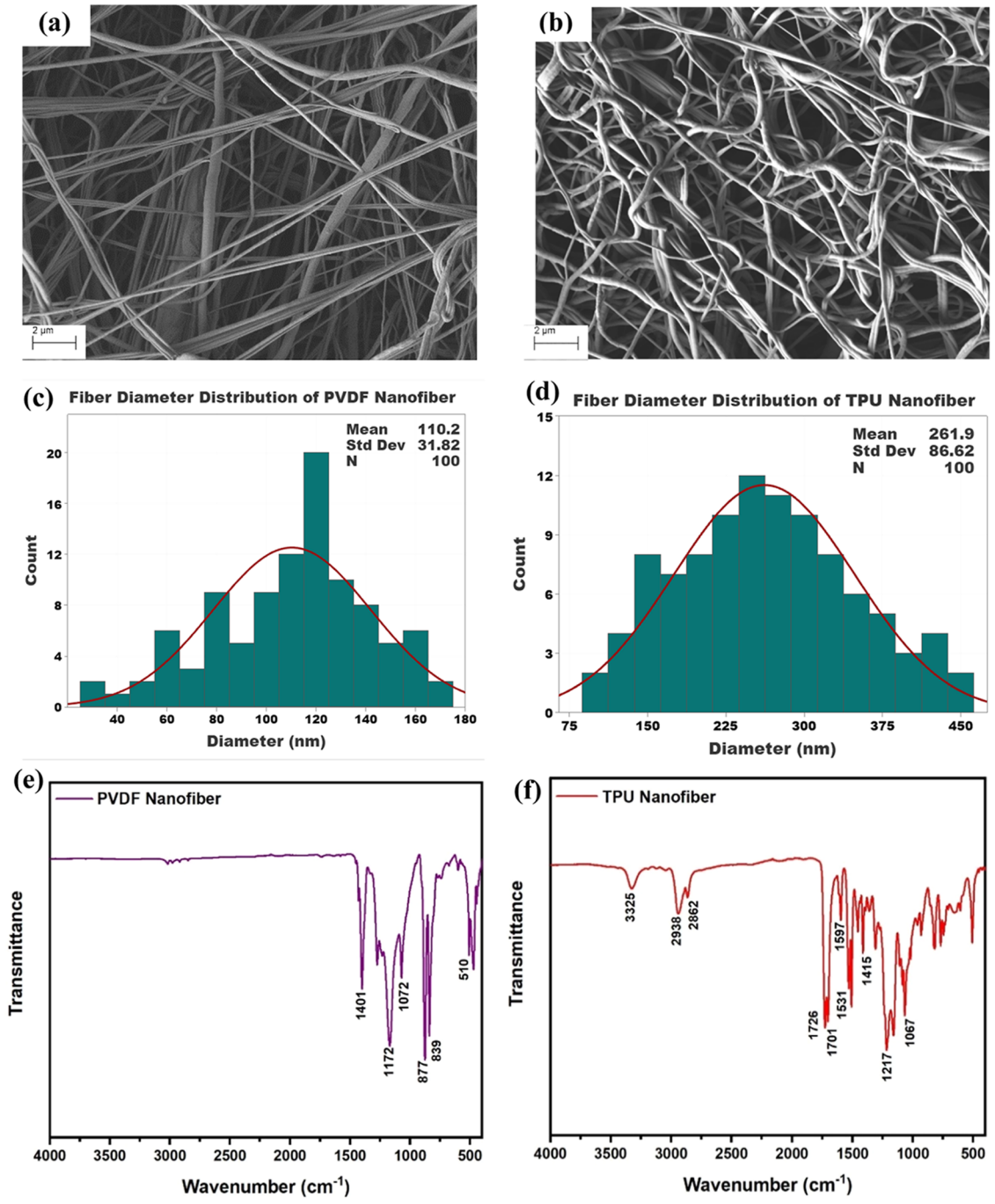

Figure 2. (a, b) FESEM images, (c, d) fiber diameter distribution histograms, and (e, f) FTIR spectrum of PVDF and TPU nanofibers.

The AFM tapping mode was used for imaging the surface morphology and roughness measurements. Silicon tips with a resonance frequency of around 300 kHz, 10 nm radius, and a spring constant of 40 N/m were selected, and measurements were carried out under ambient conditions at room temperature. Both NanoScope and WSxM software were used to analyze AFM images and to evaluate the film surface roughness of a 200 × 200 nm^2 area from each sample.

2.5. Measurement of the Output. The open-circuit output voltage of the NF-TENG was measured by a Tektronix TDS1001B digital oscilloscope, while the short-circuit current was measured by an oscilloscope connected with a Stanford Research Systems SR570 current preamplifier. The biomechanical motion responses were measured using a VersaSTAT 3 potentiostat.

3. RESULTS AND DISCUSSION

The schematics of the FS technique used to prepare the triboelectric nanofibrous membranes are illustrated in Figure 1. The morphology of the spun PVDF and TPU nanofiber can be observed in the scanning electron microscopy micrographs shown in Figure 2a,b The images show long, continuous, homogeneous, and uniform fiber surface structure. The surface morphology of PVDF NFs were found smoother, while the TPU fibers were more twisted in nature, as shown in Figures S1 and S2. From the fiber diameter histogram (Figure 2c,d), it can be accounted that the average fiber diameter of the PVDF nanofiber was ∼110 nm, while TPU nanofibers were

https://doi.org/10.1021/acsami.1c17964
ACS Appl. Mater. Interfaces 2021, 13, 60401−60412

comparatively thicker with an average fiber diameter of ~262 nm.

The nanofiber membranes were further investigated by Fourier transform infrared spectroscopy (FTIR) spectra shown in Figure 2e,f. The characteristic bands of the β phase PVDF in Figure 2e were identified in the 877, 1172, and 1401 cm^{-1} peaks. The stretching around 877 and 1072 cm^{-1} peaks was attributed to the C−C bond skeletal vibration of β PVDF[57] whereas peak at 510 cm^{-1} resulted from the $-CF_2$ bending.[58] The peaks observed at 1172 and 1401 cm^{-1} were due to the stretching vibration of C−F and C−H groups, respectively, while the band at 839 cm^{-1} was assigned to a mixed mode of $-CH_2-$ rocking and $-CF_2-$ asymmetric stretching vibration.[59] The β phase of the PVDF system promoted the triboelectric effect in the nanogenerator. The spectrum in Figure 2f revealed that the TPU membrane absorption band at 3325 cm^{-1} was due to the N−H stretching vibration in the urethane group, whereas that at 1415, 2862, and 2938 cm^{-1} corresponded to the $-CH_2-$ asymmetric stretching vibration.[60] The other characteristic sharp peaks at 1726 and 1701 cm^{-1} were associated with stretching vibration of the carbonyl group (C═O) in the amide, while stretching at 1597 cm^{-1} was caused by the N−H group flexural absorption.[61] The bands around 1067 and 1217 cm^{-1} were identified by C−O bond stretching.[62]

Fibers were imaged using the AFM tapping mode, which produces three types of images, height, deflection, and phase. Here, we present the deflection and phase images because they provide more information about the surface morphology compared to the height image. Figure 3a shows an AFM deflection image of the PVDF fiber, showing a smooth morphology made of several nanofibers clearly visible on the phase image (arrow, Figure 3b). The inset in Figure 3a shows a 3D image of the fiber where the nanofibers are visible. The average value of the roughness of the top surface of the fiber is 18 ± 2 nm (n = 10 measurements).

Figure 3c shows an AFM deflection image of the TPU fiber, showing a smooth morphology as well without any visible nanofiber as in the PVDF fiber. This is confirmed in the phase image (Figure 3d), where the top surface of the fiber looks very homogeneous. In addition, the 3D image (inset Figure 3c) does not show any specific features on the top surface of the fiber. However, the average roughness of the fiber almost doubled compared to the PVDF one, 31 ± 3 nm (n = 10 measurements). Figure 3e shows an AFM deflection image of the TPU/Au fiber, showing a homogeneous but quite different surface structure compared to the two other fibers. The presence of the nanoparticles on the surface of the fiber is clearly visible and they are homogeneously distributed. These data are confirmed with the phase image (Figure 3f), where a white structure is the most dominant. In AFM phase images, the white areas represent the harder structure that can be associated with the gold nanoparticles in our case. This is also visible in the 3D image of the fiber (inset Figure 3e). Accordingly, the average surface roughness of the fiber was also increased to 48 ± 3 nm, which added extra frictional contact during the contact and separation mechanism between the two tribo layers. Because of the geometrical convolution between the AFM tip and the shape of the fiber, only the top surface of the fiber reflects the true fiber structure.[63] Thus, the Au nanoparticles homogeneously coat the fiber. In addition, the AFM cross-sectional measurements performed on the top surface of the fiber revealed the gold layer to be around 25 ± 5 nm (n = 10 measurements).

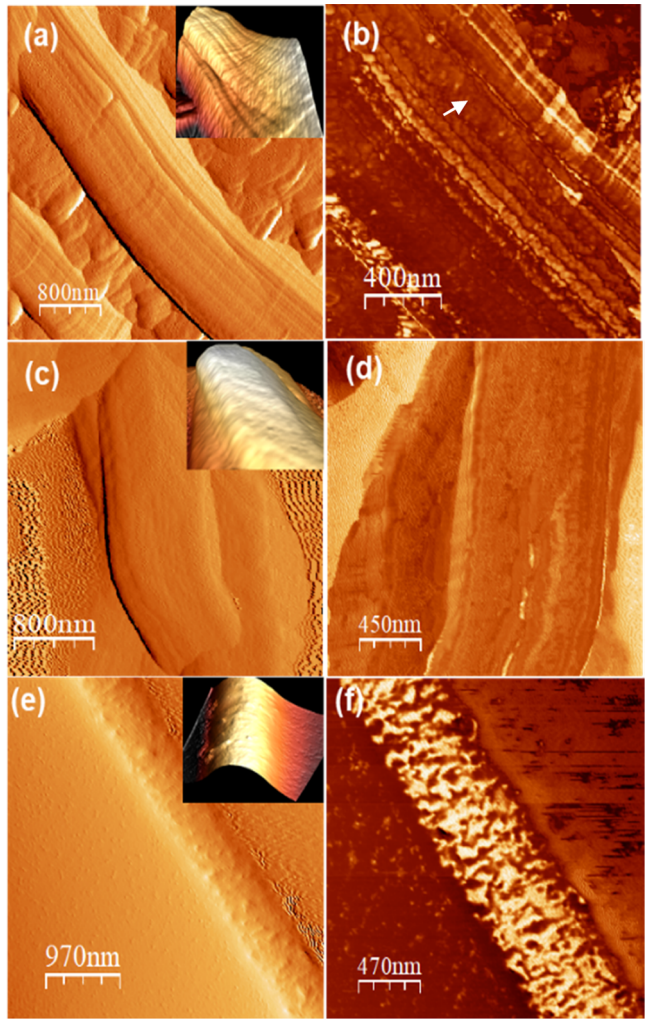

Figure 3. AFM morphology of (a, b) PVDF nanofiber, (c, d) TPU nanofiber, and (e, f) gold-sputtered TPU (TPU/Au) nanofiber.

The working principle of NF-TENG is shown in Figure S3. To produce the triboelectric effect, the TENG requires periodic vertical contact and separation, and this mechanism is imperative to the vertical contact−separation-based TENG. Owing to this continuous contact and separation, a static charge is formed on the surface of the triboelectric layers, and to maximize this charge generation, spacers are employed between the tribo layers, which makes the mechanism more convenient.[12,64] Otherwise, there is a chance of the triboelectric fiber layers to stick together during contact and separation, which might result in a lower power output. For simplicity, the spacer and PLA layers are not shown in the mechanism. Usually, a vertical contact−separation-based TENG requires two electrification layers, and initially, these two layers are in the contact mode (Figure S3a) with no current flow.[1,12] However, as the two layers are periodically pressed (come into contact and then separated) (Figure S3b), the difference in electronegativity between both layers results in charge ejection from the TPU/Au layer to the PVDF nanofiber layer.[23] The ejected electrons then resulted in net negative charges in the PVDF layer.[65] This separation induces a potential difference across the two layers, resulting in the

https://doi.org/10.1021/acsami.1c17964
ACS Appl. Mater. Interfaces 2021, 13, 60401−60412

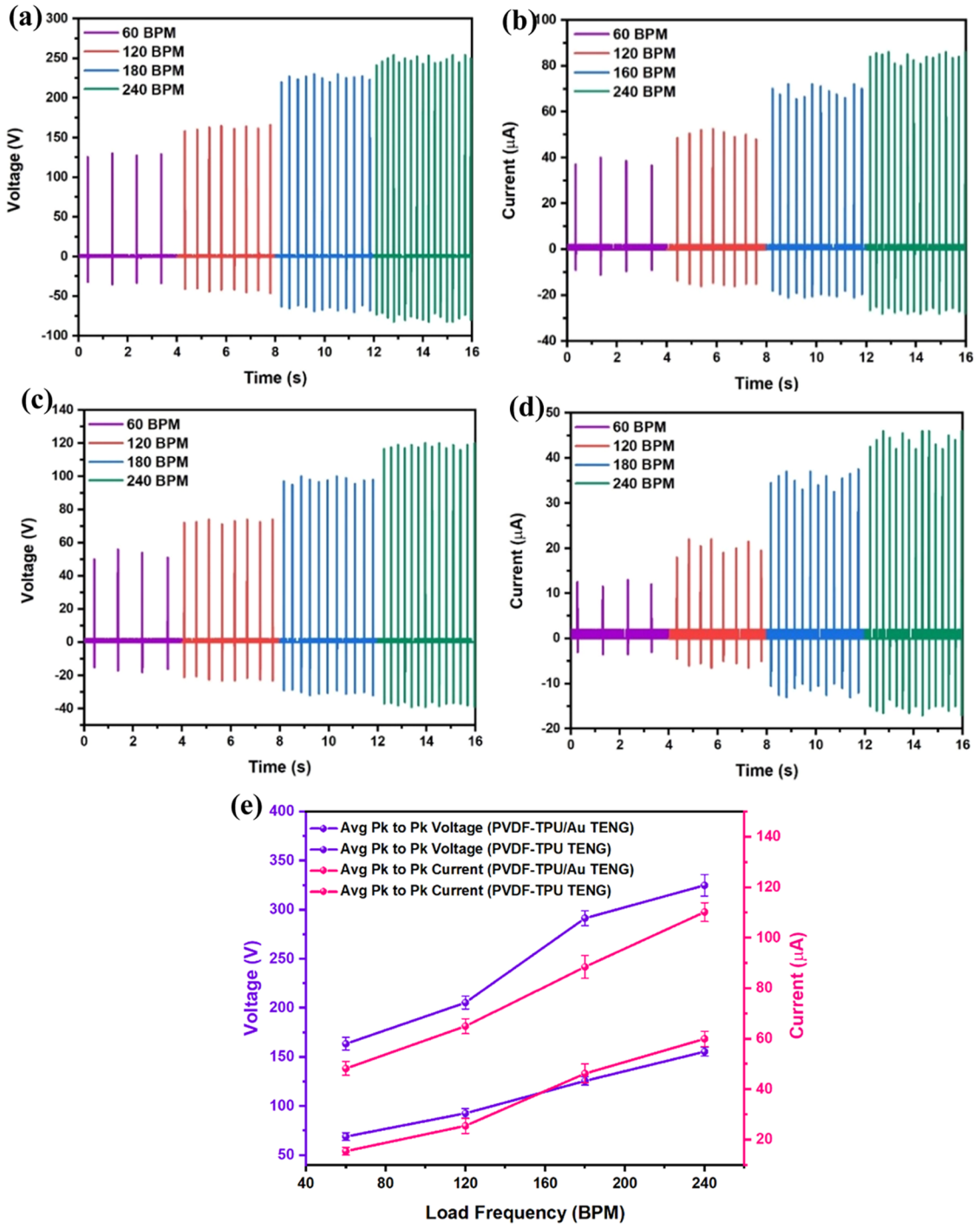

Figure 4. Electrical performance of NF-TENG. (a, c) Open-circuit voltage, (b, d) short-circuit current, and (e) average peak-to-peak voltage and current output for PVDF-TPU/Au NF-TENG and PVDF-TPU NF-TENG, respectively, for 60, 120, 180, and 240 bpm load frequencies.

current to flow through the external circuit connected to the Cu tape electrodes. When the fiber layers got fully separated (Figure S3c), the induced potential difference got balanced and the open-circuit voltage decreased and became zero.[66] When the layers were pressed again and brought closer to each other (Figure S3d), the electricity flow became reversed as the accumulated free charges flowed back.[67]

To inspect the electrical performance of PVDF-TPU/Au NF-TENG (PTA-TENG), we subjected the PTA-TENG to finger tapping at 60 bpm (1 Hz), 120 bpm (2 Hz), 180 bpm (3 Hz), and 240 bpm (4 Hz) load frequencies while keeping the range of motion to 10 cm when measured from the fingers to the top of the PTA-TENG. The vertical tapping movement of the TENG generated a triboelectric effect, which resulted in alternating current (AC) open-circuit voltage (V_{OC}) and short-circuit current (I_{SC}), as shown in Figure 4. The results indicate that both V_{OC} and I_{SC} increased with increasing load frequency.[68] The maximum V_{OC} recorded for PTA-TENG was 130, 165, 230, and 254 V (Figure 4a) for 60, 120, 180, and 240 bpm load frequency, respectively, while the highest I_{SC} obtained were 42, 52.5, 72, and 86 μA (Figure 4b) for 60, 120, 180, and 240 bpm. The outputs were then compared with the

https://doi.org/10.1021/acsami.1c17964
ACS Appl. Mater. Interfaces 2021, 13, 60401−60412

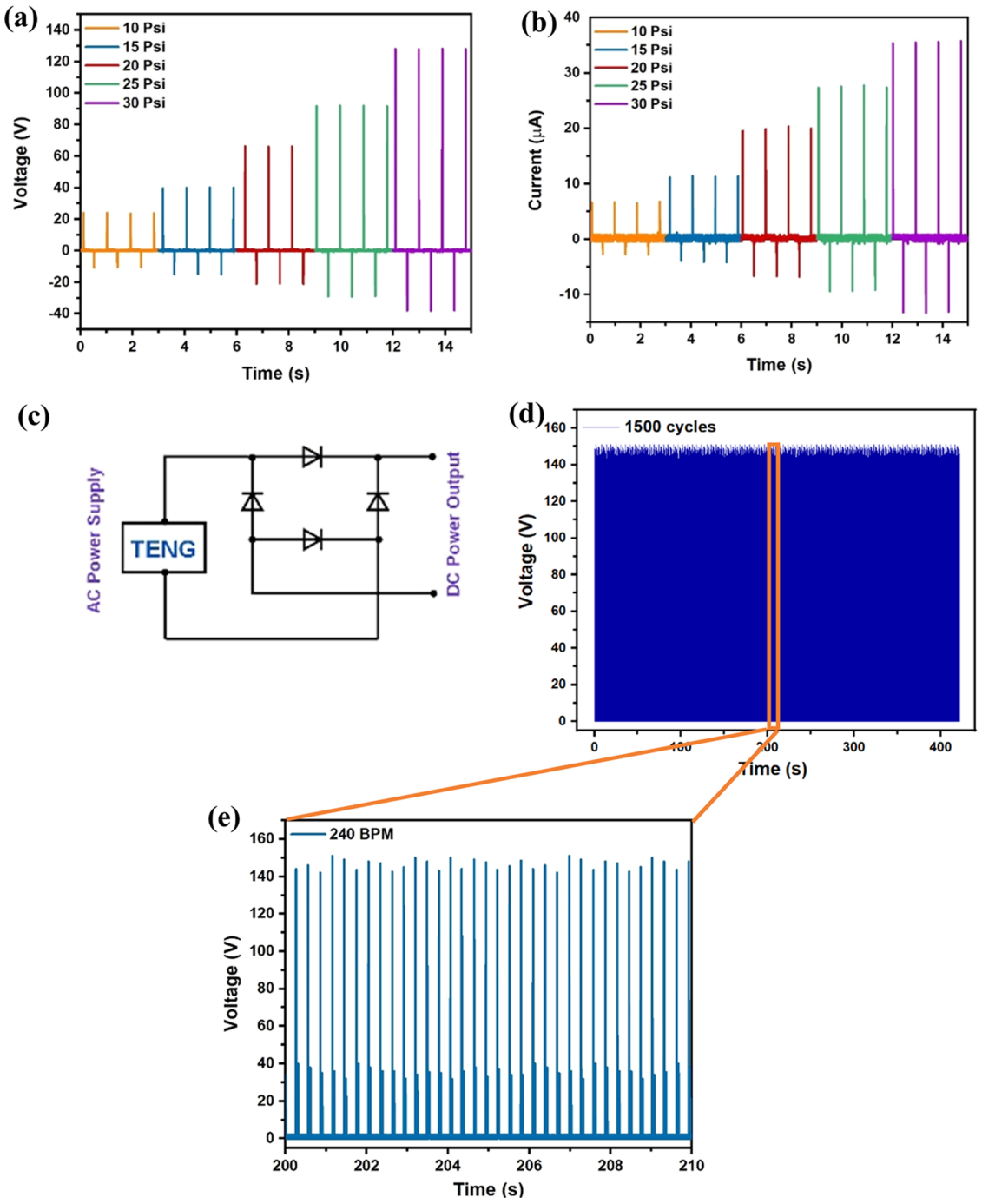

Figure 5. Electrical performance of PTA-TENG. (a) Open-circuit voltage and (b) short-circuit current output for different pressures at a 65 bpm load frequency. (c) Full-bridge rectifier circuit. (d) Stability and durability test of the rectified PTA-TENG under periodic contact−separation processes for 1500 cycles and (e) enlarged view of the response during load cycles at a 240 bpm load frequency.

bare PVDF-TPU nanofiber-based TENG, as shown in Figure 4c,d. The highest AC open-circuit voltage and short-circuit current recorded were 120 V and 46 μA at a 240 bpm load frequency, which signified that the effect of Au on the surface of TPU nanofiber improved the output performance by ∼112 and ∼86%, respectively, for open-circuit voltage and short-circuit current. From Figure 4e, it can be interpreted that the highest average peak-to-peak voltage and current achieved for gold-sputtered TPU-based TENG were 329 ± 7 V and 110.25 ± 3.75 μA, which were significantly higher than normal TPU-PVDF nanofiber-based TENG, which yielded only 155.5 ± 3.5 V and 60 ± 3 μA at a 240 bpm load frequency.

Moreover, to further investigate the PTA-TENG performance with constant pressure, we used a vertical force machine (Figure S4), where we varied the load from 10 to 30 psi at a 65 bpm frequency (Figure 5); the output signal showed similar results like those observed in finger tapping but this time the resulting peaks showed higher uniformity. As the applied pressure increased, the force of impact increased on the triboelectric surface and the output AC V_{OC} values observed were 24, 40, 66, 92, and 128 V for 10, 15, 20, 25, and 35 psi

https://doi.org/10.1021/acsami.1c17964
ACS Appl. Mater. Interfaces 2021, 13, 60401−60412

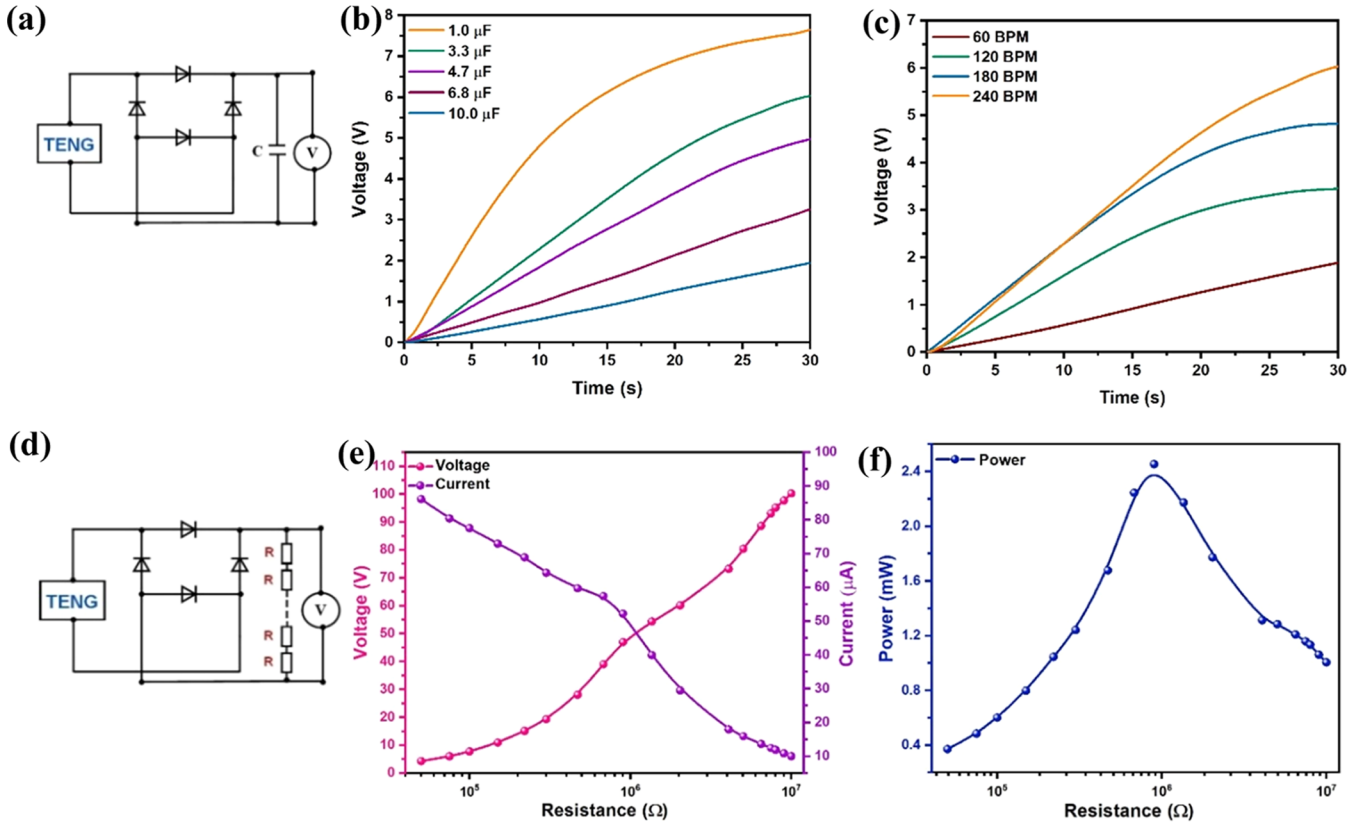

Figure 6. Electrical performance of PTA-TENG. (a) Capacitor test circuit, (b) charging ability of NF-TENG with different capacitors, (c) charging with a 3.3 μF capacitor for different bpm load frequencies. (d) Resistance test circuit, (e) average voltage and current, and (f) power output of PTA-TENG with different external resistances.

(Figure 5a), respectively. In addition, the output current signals were also increased linearly and yielded 6.7, 11.4, 20.35, 27.75, and 35.6 μA short-circuit current for 10, 15, 20, 25, and 30 psi, respectively (Figure 5b). However, the output V_{OC} and I_{SC} achieved during the pressure test were quite smaller compared to the finger-tapping test as the effective contact area was only 5.07 cm^2 with the circular piston having a diameter of 2.54 cm (Figure S4), while during finger tapping, the active triboelectric surface area was 8 cm^2 (3.2 × 2.5 cm^2). Figure 5c shows the schematic of the full-wave bridge rectifier circuit. Consequently, the durability performance of the PTA-TENG was also examined under periodic contact−separation operation for 1500 cycles at a 240 bpm load frequency, and the results strongly illustrate the long stability of our proposed TENG where the maximum rectified voltage was recorded at 152 V (Figure 5e).

In contrast to electrical performance, the charging ability of the PTA-TENG was also investigated with different capacitors to demonstrate future prospects of storing and charging small electronic devices. Figure 6a shows the schematic view of the capacitor circuit with a full-wave bridge rectifier attached to the TENG used in the experiment. The capacitor with 1.0, 3.3, 4.7, 6.8, and 10.0 μF capacitance was employed for charging for 30 s at a 240 bpm load frequency with finger tapping (Figure 6b). The curves show that as the capacitance increased, the rate of charging capacity gradually decreased. The maximum output voltages observed for the abovementioned capacitors were 7.64, 6.03, 4.97, 3.26, and 1.95 V, respectively. Furthermore, after examining different capacitors, the PTA-TENG was further experimented with a 3.3 μF capacitor but this time with varying load frequencies.

From Figure 6c, it can be highlighted that for a constant 30s tapping mode, the output voltage got higher as the load frequency varied from 60 to 240 bpm. The highest voltage was recorded to be 6.03 V at 240 bpm where a 60 bpm load frequency derived only 1.89 V, which illustrated that higher voltage can be achieved with high load frequency.[69] Figure 6d shows the external resistance load connected in series with the full-wave bridge-rectified nanogenerator. From Figure 6e, it can be elucidated that the instantaneous average voltage output showed a gradual increase, while the average current output indicated an opposite trend with varying resistive loads from 50 kΩ to 10 MΩ at a frequency of 4 Hz (240 bpm) following Ohm's law.[65]

According to the maximum power transfer theorem, the maximum power output is achieved when the internal impedance of the TENG is in sync with the external load.[21] A sharp increase in the voltage output was observed from 0.47 to 0.9 MΩ. As a result, the power ($P = V^2/R$) initially increased (Figure 6f) and reached a maximum of ∼2.45 mW at a 0.9 MΩ load resistance and then gradually started to decrease. Moreover, to demonstrate the feasibility of our nanogenerator, we illuminated 75 LED with high brightness. The TENG was attached with a series of commercial LEDs (1.5 V each) through a full-wave bridge rectifier with a 0.1 μF capacitor and the nanogenerator was hand tapped to light up the LEDs (Figure S5). This high-power output and the LED test of the PTA-TENG demonstrated promising potential to power flexible and wearable electronics.[64,70]

https://doi.org/10.1021/acsami.1c17964
ACS Appl. Mater. Interfaces 2021, 13, 60401−60412

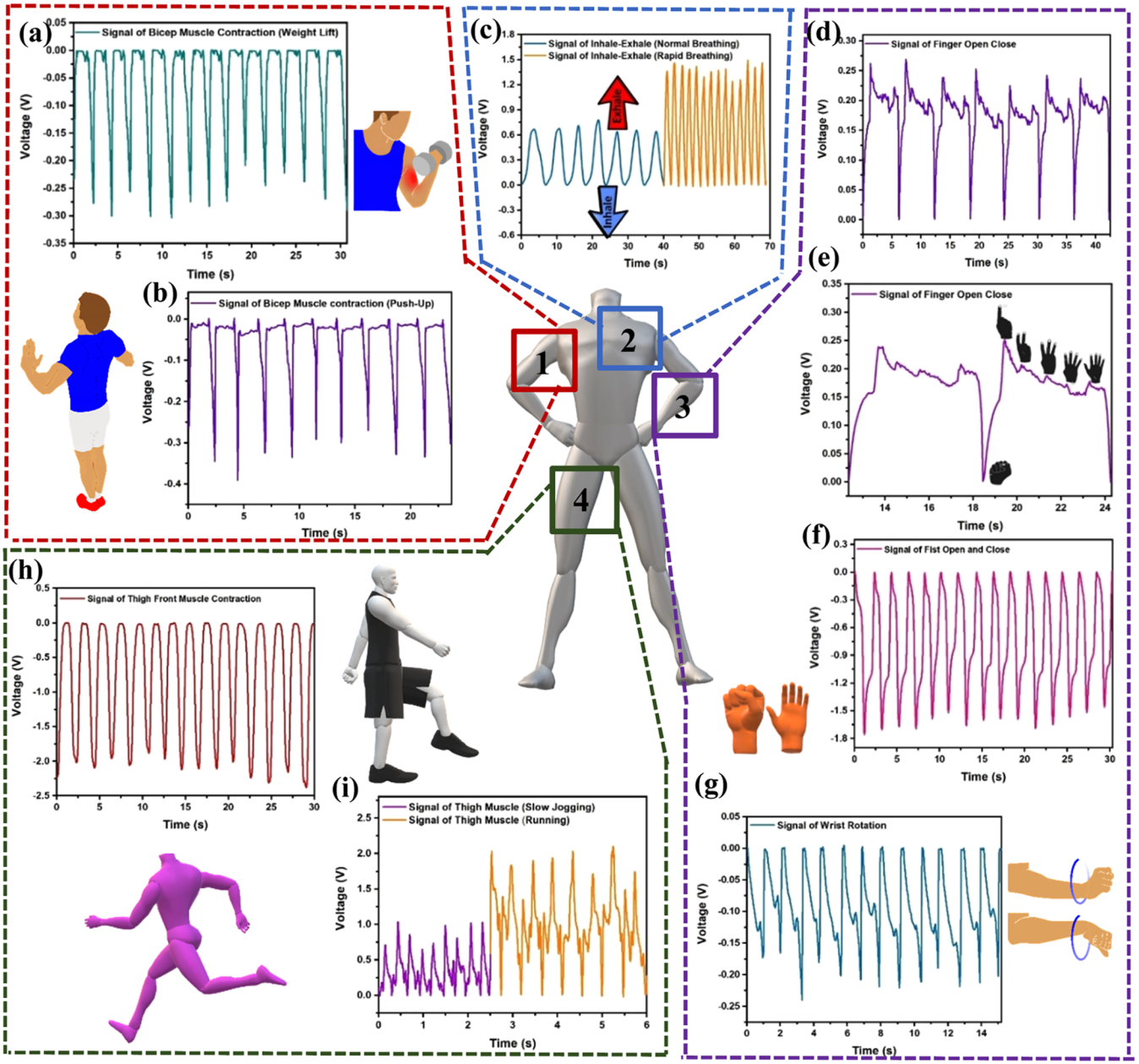

Figure 7. Sensing performance of PTA-TENG for different body motions. The signal of bicep muscle contraction for (a) 5 lb weight lift and (b) incline push up. (c) Signal of normal breathing and rapid breathing. The signal from the forearm for (d) finger's gradual opening and closing, (e) magnified signal of finger opening and closing, (f) fist opening and closing, and (g) wrist rotation. The thigh muscle (quadricep) contraction signal for (h) leg up−down movement and (i) slow jogging and running.

After investigating the energy-storage capability of PTA-TENG, the nanogenerator was explored for various bio-mechanical motion-sensing applications, as shown in Figure 7. During the 5lb weight lift (Figure 7a) and incline push up (Figure 7b), the bicep muscle contraction was recorded as an AC open-circuit voltage signal (~0.25 to 0.35 V peak), which signified superior bending sense capability of the proposed sensor. The sensor was further examined to detect the respiration rate at normal breathing and rapid breathing during running (Figure 7c). The results show a sinusoidal signal for the inhalation and exhalation motion by attaching the TENG at the chest. As the sensor was prepared by a nanofiber, air could easily penetrate the fiber membrane. Similar to bicep contraction, the PTA-TENG sensor was also investigated for different hand gestures: one by one finger opening and then closing altogether (Figure 7d) and fist opening and closing (Figure 7f) at a 1 Hz frequency. The distinct peak in the figure (Figure 7e) clearly showed how many fingers were opened or closed at a given time. The output voltage signals were generated by the pressure drop across two friction TENG layers. The fist opening and closing responses were repetitive (~1.8 V peak) and distinctive, and moreover, the output looked like a twisted pulsed signal. The forearm muscle contraction test was also performed for wrist rotation (clockwise direction), as shown in Figure 7g, at a 60 bpm load frequency and a similar pattern of the signal was depicted at a regular time interval.

The TENG sensor was then attached to the front part of the leg, just above the knee, and near the quadricep muscles to capture the motion of the muscle contraction and expansion.

https://doi.org/10.1021/acsami.1c17964
ACS Appl. Mater. Interfaces 2021, 13, 60401−60412

The results from the bending of the leg to 90 degrees from the standing position, as shown in Figure 7h, were quite similar to bicep contraction, but the peaks were intense (~2.4 V). The quadricep contraction was also captured during slow jogging and running, as shown in Figure 7i. In both cases, the signals were the same but only varied in respect to V_{OC} peak intensity, as in the case of running, the V_{OC} peaks were ~2.0 V, double than slow jogging. The reaction from different body motion gestures clearly indicated real-life self-power sensor capability. Consequently, our proposed PTA-TENG was able to evaluate physiological information meticulously while charging small electronics simultaneously.

4. CONCLUSIONS

In summary, we have fabricated for the first time a triboelectric nanogenerator with PVDF and TPU nanofibers prepared by the FS technique. The spun nanofiber layer improved electrification properties due to the β phase domination in the PVDF nanofiber, which resulted from the unidirectional mechanical stretching during fiber formation. However, to upgrade the performance of the triboelectric response, we sputtered gold coating over the TPU nanofiber surface. This simple surface modification with an additional frictional surface resulted in a noticeable electrical output of a 254 V open-circuit voltage and a 86 μA short-circuit current, which were 2.12 and 1.87 times greater than bare TPU/PVDF nanofiber-based TENG. Constant pressure tests were also conducted to illustrate the capability of a uniform signal output in comparison to the finger-tapping mode. The capacitor charging test of the modified TENG offered a quick charging capability of a maximum of 7.64 V within 30 s using a 1.0 μF capacitor, which indicates the great promise of our TENG for charging small electronics. Furthermore, attaching external resistance load and varying it from 50 kΩ to 10 MΩ, we obtained significant 2.45 mW power from a small TENG with an active contact area of only 8.0 cm^2, which eventually implied prospects of our prepared TENG for a small but high-density power source. The real-life applicability of the TENG was explored by illuminating 75 commercial LEDs by only 12 s of hand tapping. The nanogenerator was further analyzed for sensory application by connecting to different body parts, namely, forearm, quadricep muscle, and chest, and it demonstrated an attractive capability for distinct human biomechanical motion-sensing application.

■ ASSOCIATED CONTENT

Supporting Information

The Supporting Information is available free of charge at https://pubs.acs.org/doi/10.1021/acsami.1c17964.

Figures S1 and S2: FESEM images at 2.0, 3.0, and 5.0 magnification for PVDF and TPU nanofibers, Figure S3: contact−separation working mechanism of the PTA-TENG and the three-dimensional (3D) scheme of the TENG cell, Figure S4: experimental setup of the fixed pressure test machine, and Figure S5: schematic circuit diagram of the LED test and photographic representation of lighting up LED by hand-tapping motion (PDF)

■ AUTHOR INFORMATION

Corresponding Authors

Mohammed Jasim Uddin − *Photonics and Energy Research Laboratory and Department of Chemistry, University of Texas Rio Grande Valley, Edinburg, Texas 78539, United States;* orcid.org/0000-0002-7935-7269; Email: mohammed.uddin@utrgv.edu

Karen Lozano − *Center for Nanotechnology, Department of Mechanical Engineering, University of Texas Rio Grande Valley, Edinburg, Texas 78539, United States;* orcid.org/0000-0002-6676-8632; Email: karen.lozano@utrgv.edu

Authors

Sk Shamim Hasan Abir − *Photonics and Energy Research Laboratory and Center for Nanotechnology, Department of Mechanical Engineering, University of Texas Rio Grande Valley, Edinburg, Texas 78539, United States*

Muhtasim Ul Karim Sadaf − *Photonics and Energy Research Laboratory and Department of Chemistry, University of Texas Rio Grande Valley, Edinburg, Texas 78539, United States*

Sunanda Kumar Saha − *Center for Nanotechnology, Department of Mechanical Engineering, University of Texas Rio Grande Valley, Edinburg, Texas 78539, United States*

Ahmed Touhami − *Department of Physics and Astronomy, University of Texas Rio Grande Valley, Brownsville, Texas 78520, United States*

Complete contact information is available at: https://pubs.acs.org/10.1021/acsami.1c17964

Author Contributions

This manuscript was written by S.S.H.A., A.T., and M.U.K.S. The experiments were performed by S.S.H.A., M.U.K.S., and S.K.S. K.L., M.J.U., and A.T. edited and revised the final manuscript. M.J.U. and K.L. supervised the project. All of the authors have given their approval to the final version of the manuscript.

Notes

The authors declare no competing financial interest.

■ ACKNOWLEDGMENTS

The authors gratefully acknowledge support received by the NSF PREM award under Grant No. DMR 2122178-: UTRGV-UMN Partnership to Strengthen the PREM Pathway. M.K.S. gratefully acknowledges the support from the UTRGV Presidential Graduate Fellowship and Welch Foundation Research (Grant No. BX 0048).

■ REFERENCES

(1) Qiu, H. J.; Song, W. Z.; Wang, X. X.; Zhang, J.; Fan, Z.; Yu, M.; Ramakrishna, S.; Long, Y. Z. A Calibration-Free Self-Powered Sensor for Vital Sign Monitoring and Finger Tap Communication Based on Wearable Triboelectric Nanogenerator. *Nano Energy* **2019**, *58*, 536−542.

(2) Zhao, S.; Wang, J.; Du, X.; Wang, J.; Cao, R.; Yin, Y.; Zhang, X.; Yuan, Z.; Xing, Y.; Pui, D. Y. H.; Li, C. All-Nanofiber-Based Ultralight Stretchable Triboelectric Nanogenerator for Self-Powered Wearable Electronics. *ACS Appl. Energy Mater.* **2018**, *1*, 2326−2332.

(3) Liu, W.; Song, M. S.; Kong, B.; Cui, Y. Flexible and Stretchable Energy Storage: Recent Advances and Future Perspectives. *Adv. Mater.* **2017**, *29*, No. 1603436.

(4) Armand, M. Issues and challenges facing rechargeable lithium batteries. *Nature* **2001**, *414*, 359−367.

(5) Wang, Y.; Yang, Y.; Wang, Z. L. Triboelectric Nanogenerators as Flexible Power Sources. *npj Flex. Electron.* **2017**, *1*, No. 10.

(6) Huang, T.; Wang, C.; Yu, H.; Wang, H.; Zhang, Q.; Zhu, M. Human Walking-Driven Wearable All-Fiber Triboelectric Nano-

generator Containing Electrospun Polyvinylidene Fluoride Piezoelectric Nanofibers. *Nano Energy* **2015**, *14*, 226−235.
(7) Zi, Y.; Lin, L.; Wang, J.; Wang, S.; Chen, J.; Fan, X.; Yang, P. K.; Yi, F.; Wang, Z. L. Triboelectric-Pyroelectric-Piezoelectric Hybrid Cell for High-Efficiency Energy-Harvesting and Self-Powered Sensing. *Adv. Mater.* **2015**, *27*, 2340−2347.
(8) Kim, Y.; Wu, X.; Oh, J. H. Fabrication of Triboelectric Nanogenerators Based on Electrospun Polyimide Nanofibers Membrane. *Sci. Rep.* **2020**, *10*, No. 2742.
(9) Wang, Z. L. From Contact Electrification to Triboelectric Nanogenerators. *Rep. Prog. Phys.* **2021**, *84*, No. 096502.
(10) Fan, F. R.; Tian, Z. Q.; Lin Wang, Z. Flexible Triboelectric Generator. *Nano Energy* **2012**, *1*, 328−334.
(11) Zou, H.; Zhang, Y.; Guo, L.; Wang, P.; He, X.; Dai, G.; Zheng, H.; Chen, C.; Wang, A. C.; Xu, C.; Wang, Z. L. Quantifying the Triboelectric Series. *Nat. Commun.* **2019**, *10*, No. 1427.
(12) Abdullah, A. M.; Sadaf, M. U. K.; Tasnim, F.; Vasquez, H.; Lozano, K.; Uddin, M. J. KNN Based Piezo-Triboelectric Lead-Free Hybrid Energy Films. *Nano Energy* **2021**, *86*, No. 106133.
(13) Shawon, S. M. A. Z.; Sun, A. X.; Vega, V. S.; Chowdhury, B. D.; Tran, P.; Carballo, Z. D.; Tolentino, J. A.; Li, J.; Rafaqut, M. S.; Danti, S.; Uddin, M. J. Piezo-Tribo Dual Effect Hybrid Nanogenerators for Health Monitoring. *Nano Energy* **2021**, *82*, No. 105691.
(14) Lopez, D.; Chowdhury, A. R.; Abdullah, A. M.; Sadaf, M. U. K.; Martinez, I.; Choudhury, B. D.; Danti, S.; Ellison, C. J.; Lozano, K.; Uddin, M. J. Polymer Based Triboelectric Nanogenerator for Cost-Effective Green Energy Generation and Implementation of Surface-Charge Engineering. *Energy Technol.* **2021**, *9*, No. 2001088.
(15) Yu, B.; Yu, H.; Huang, T.; Wang, H.; Zhu, M. A Biomimetic Nanofiber-Based Triboelectric Nanogenerator with an Ultrahigh Transfer Charge Density. *Nano Energy* **2018**, *48*, 464−470.
(16) Bhatta, T.; Maharjan, P.; Cho, H.; Park, C.; Yoon, S. H.; Sharma, S.; Salauddin, M.; Rahman, M. T.; Rana, S. S.; Park, J. Y. High-Performance Triboelectric Nanogenerator Based on MXene Functionalized Polyvinylidene Fluoride Composite Nanofibers. *Nano Energy* **2021**, *81*, No. 105670.
(17) Zhang, J. H.; Li, Y.; Du, J.; Hao, X.; Huang, H. A High-Power Wearable Triboelectric Nanogenerator Prepared from Self-Assembled Electrospun Poly(Vinylidene Fluoride) Fibers with a Heart-like Structure. *J. Mater. Chem. A* **2019**, *7*, 11724−11733.
(18) Dudem, B.; Kim, D. H.; Mule, A. R.; Yu, J. S. Enhanced Performance of Microarchitectured PTFE-Based Triboelectric Nanogenerator via Simple Thermal Imprinting Lithography for Self-Powered Electronics. *ACS Appl. Mater. Interfaces* **2018**, *10*, 24181−24192.
(19) Yu, J.; Hou, X.; Cui, M.; Shi, S.; He, J.; Sun, Y.; Wang, C.; Chou, X. Flexible PDMS-Based Triboelectric Nanogenerator for Instantaneous Force Sensing and Human Joint Movement Monitoring. *Sci. China Mater.* **2019**, *62*, 1423−1432.
(20) Wang, X.; Yang, B.; Liu, J.; Zhu, Y.; Yang, C.; He, Q. A Flexible Triboelectric-Piezoelectric Hybrid Nanogenerator Based on P(VDF-TrFE) Nanofibers and PDMS/MWCNT for Wearable Devices. *Sci. Rep.* **2016**, *6*, No. 36409.
(21) Wu, Y.; Qu, J.; Daoud, W. A.; Wang, L.; Qi, T. Flexible Composite-Nanofiber Based Piezo-Triboelectric Nanogenerators for Wearable Electronics. *J. Mater. Chem. A* **2019**, *7*, 13347−13355.
(22) Zhang, C.; Zhou, T.; Tang, W.; Han, C.; Zhang, L.; Wang, Z. L. Rotating-Disk-Based Direct-Current Triboelectric Nanogenerator. *Adv. Energy Mater.* **2014**, *4*, No. 1301798.
(23) Oh, H. J.; Bae, J. H.; Park, Y. K.; Song, J.; Kim, D. K.; Lee, W.; Kim, M.; Heo, K. J.; Kim, Y.; Kim, S. H.; Yeang, B. J.; Lim, S. J. A Highly Porous Nonwoven Thermoplastic Polyurethane/Polypropylene-Based Triboelectric Nanogenerator for Energy Harvesting by Human Walking. *Polymers* **2020**, *12*, No. 1044.
(24) Yar, A.; Karabiber, A.; Ozen, A.; Ozel, F.; Coskun, S. Flexible Nanofiber Based Triboelectric Nanogenerators with High Power Conversion. *Renewable Energy* **2020**, *162*, 1428−1437.
(25) Cui, S.; Zheng, Y.; Liang, J.; Wang, D. Triboelectrification Based on Double-Layered Polyaniline Nanofibers for Self-Powered Cathodic Protection Driven by Wind. *Nano Res.* **2018**, *11*, 1873−1882.
(26) Zheng, Y.; Cheng, L.; Yuan, M.; Wang, Z.; Zhang, L.; Qin, Y.; Jing, T. An Electrospun Nanowire-Based Triboelectric Nanogenerator and Its Application in a Fully Self-Powered UV Detector. *Nanoscale* **2014**, *6*, 7842−7846.
(27) Peng, X.; Dong, K.; Ye, C.; Jiang, Y.; Zhai, S.; Cheng, R.; Liu, D.; Gao, X.; Wang, J.; Wang, Z. L. A Breathable, Biodegradable, Antibacterial, and Self-Powered Electronic Skin Based on All-Nanofiber Triboelectric Nanogenerators. *Sci. Adv.* **2020**, *6*, No. eaba9624.
(28) Wang, S.; Tai, H.; Liu, B.; Duan, Z.; Yuan, Z.; Pan, H.; Su, Y.; Xie, G.; Du, X.; Jiang, Y. A Facile Respiration-Driven Triboelectric Nanogenerator for Multifunctional Respiratory Monitoring. *Nano Energy* **2019**, *58*, 312−321.
(29) Syu, M. H.; Guan, Y. J.; Lo, W. C.; Fuh, Y. K. Biomimetic and Porous Nanofiber-Based Hybrid Sensor for Multifunctional Pressure Sensing and Human Gesture Identification via Deep Learning Method. *Nano Energy* **2020**, *76*, No. 105029.
(30) Huang, T.; Yu, H.; Wang, H.; Zhang, Q.; Zhu, M. Hydrophobic SiO2 Electret Enhances the Performance of Poly(Vinylidene Fluoride) Nanofiber-Based Triboelectric Nanogenerator. *J. Phys. Chem. C* **2016**, *120*, 26600−26608.
(31) Gu, G. Q.; Han, C. B.; Tian, J. J.; Jiang, T.; He, C.; Lu, C. X.; Bai, Y.; Nie, J. H.; Li, Z.; Wang, Z. L. Triboelectric Nanogenerator Enhanced Multilayered Antibacterial Nanofiber Air Filters for Efficient Removal of Ultrafine Particulate Matter. *Nano Res.* **2018**, *11*, 4090−4101.
(32) Mi, H. Y.; Jing, X.; Zheng, Q.; Fang, L.; Huang, H. X.; Turng, L. S.; Gong, S. High-Performance Flexible Triboelectric Nanogenerator Based on Porous Aerogels and Electrospun Nanofibers for Energy Harvesting and Sensitive Self-Powered Sensing. *Nano Energy* **2018**, *48*, 327−336.
(33) Huang, T.; Lu, M.; Yu, H.; Zhang, Q.; Wang, H.; Zhu, M. Enhanced Power Output of a Triboelectric Nanogenerator Composed of Electrospun Nanofiber Mats Doped with Graphene Oxide. *Sci. Rep.* **2015**, *5*, No. 13942.
(34) Liu, J.; Zhang, L.; Wang, N.; Li, C. Highly Stretchable and Transparent Triboelectric Nanogenerator Based on Multilayer Structured Stable Electrode for Self-Powered Wearable Sensor. *Nano Energy* **2020**, *78*, No. 105385.
(35) Xu, H.; Xiang, J. X.; Lu, Y. F.; Zhang, M. K.; Li, J. J.; Gao, B. B.; Zhao, Y. J.; Gu, Z. Z. Multifunctional Wearable Sensing Devices Based on Functionalized Graphene Films for Simultaneous Monitoring of Physiological Signals and Volatile Organic Compound Biomarkers. *ACS Appl. Mater. Interfaces* **2018**, *10*, 11785−11793.
(36) Huang, P.; Wen, D. L.; Qiu, Y.; Yang, M. H.; Tu, C.; Zhong, H. S.; Zhang, X. S. Textile-Based Triboelectric Nanogenerators for Wearable Self-Powered Microsystems. *Micromachines* **2021**, *12*, No. 158.
(37) Khan, Y.; Garg, M.; Gui, Q.; Schadt, M.; Gaikwad, A.; Han, D.; Yamamoto, N. A. D.; Hart, P.; Welte, R.; Wilson, W.; Czarnecki, S.; Poliks, M.; Jin, Z.; Ghose, K.; Egitto, F.; Turner, J.; Arias, A. C. Flexible Hybrid Electronics: Direct Interfacing of Soft and Hard Electronics for Wearable Health Monitoring. *Adv. Funct. Mater.* **2016**, *26*, 8764−8775.
(38) Alam, M. M.; Lee, S.; Kim, M.; Han, K. S.; Cao, V. A.; Nah, J. Ultra-Flexible Nanofiber-Based Multifunctional Motion Sensor. *Nano Energy* **2020**, *72*, No. 104672.
(39) Qin, Z.; Chen, X.; Yin, Y.; Ma, G.; Jia, Y.; Deng, J.; Pan, K. Flexible Janus Electrospun Nanofiber Films for Wearable Triboelectric Nanogenerator. *Adv. Mater. Technol.* **2020**, *5*, No. 1900859.
(40) Abir, S. S. H.; Hasan, M. T.; Alcoutlabi, M.; Lozano, K. The Effect of Solvent and Molecular Weight on the Morphology of Centrifugally Spun Poly(Vinylpyrrolidone) Nanofibers. *Fibers Polym.* **2021**, *22*, 2394−2403.
(41) Hasan, M. T.; Gonzalez, R.; Chipara, M.; Materon, L.; Parsons, J.; Alcoutlabi, M. Antibacterial Activities of Centrifugally Spun

Polyethylene Oxide/Silver Composite Nanofibers. *Polym. Adv. Technol.* **2021**, *32*, 2327−2338.
(42) Abir, S. S. H.; Gupta, S. K.; Ibrahim, A.; Srivastava, B. B.; Lozano, K. Tunable CsPb(Br/Cl)3 Perovskite Nanocrystals and Further Advancement in Designing Light Emitting Fiber Membranes. *Mater. Adv.* **2021**, *2*, 2700−2710.
(43) Trevino, J. E.; Mohan, S.; Salinas, A. E.; Cueva, E.; Lozano, K. Piezoelectric Properties of PVDF-Conjugated Polymer Nanofibers. *J. Appl. Polym. Sci.* **2021**, *138*, No. 50665.
(44) Mi, H. Y.; Jing, X.; Meador, M. A. B.; Guo, H.; Turng, L. S.; Gong, S. Triboelectric Nanogenerators Made of Porous Polyamide Nanofiber Mats and Polyimide Aerogel Film: Output Optimization and Performance in Circuits. *ACS Appl. Mater. Interfaces* **2018**, *10*, 30596−30606.
(45) Hao, Y.; Bin, Y.; Tao, H.; Cheng, W.; Hongzhi, W.; Meifang, Z. In *Preparation and Optimization of Polyvinylidene Fluoride (PVDF) Triboelectric Nanogenerator via Electrospinning*, IEEE-NANO 2015 − 15th International Conference on Nanotechnology, 2015.
(46) Wu, J. L.; Chen, F. C.; Hsiao, Y. S.; Chien, F. C.; Chen, P.; Kuo, C. H.; Huang, M. H.; Hsu, C. S. Surface Plasmonic Effects of Metallic Nanoparticles on the Performance of Polymer Bulk Heterojunction Solar Cells. *ACS Nano* **2011**, *5*, 959−967.
(47) Amarandei, G.; O'Dwyer, C.; Arshak, A.; Corcoran, D. Fractal Patterning of Nanoparticles on Polymer Films and Their SERS Capabilities. *ACS Appl. Mater. Interfaces* **2013**, *5*, 8655−8662.
(48) Bi, Y. G.; Feng, J.; Liu, Y. S.; Li, Y. F.; Chen, Y.; Zhang, X. L.; Han, X. C.; Sun, H. B. Surface Plasmon-Polariton Mediated Red Emission from Organic Light-Emitting Devices Based on Metallic Electrodes Integrated with Dual-Periodic Corrugation. *Sci. Rep.* **2014**, *4*, No. 7108.
(49) Schwartzkopf, M.; Santoro, G.; Brett, C. J.; Rothkirch, A.; Polonskyi, O.; Hinz, A.; Metwalli, E.; Yao, Y.; Strunskus, T.; Faupel, F.; Müller-Buschbaum, P.; Roth, S. V. Real-Time Monitoring of Morphology and Optical Properties during Sputter Deposition for Tailoring Metal-Polymer Interfaces. *ACS Appl. Mater. Interfaces* **2015**, *7*, 13547−13556.
(50) Schwartzkopf, M.; Wöhnert, S. J.; Waclawek, V.; Carstens, N.; Rothkirch, A.; Rubeck, J.; Gensch, M.; Drewes, J.; Polonskyi, O.; Strunskus, T.; Hinz, A. M.; Schaper, S. J.; Körstgens, V.; Müller-Buschbaum, P.; Faupel, F.; Roth, S. V. Real-Time Insight into Nanostructure Evolution during the Rapid Formation of Ultra-Thin Gold Layers on Polymers. *Nanoscale Horiz.* **2021**, *6*, 132−138.
(51) Schwartzkopf, M.; Hinz, A.; Polonskyi, O.; Strunskus, T.; Löhrer, F. C.; Körstgens, V.; Müller-Buschbaum, P.; Faupel, F.; Roth, S. V. Role of Sputter Deposition Rate in Tailoring Nanogranular Gold Structures on Polymer Surfaces. *ACS Appl. Mater. Interfaces* **2017**, *9*, 5629−5637.
(52) Roth, S. V.; Döhrmann, R.; Gehrke, R.; Röhlsberger, R.; Schlage, K.; Metwalli, E.; Körstgens, V.; Burghammer, M.; Riekel, C.; David, C.; Müller-Buschbaum, P. Mapping the Morphological Changes of Deposited Gold Nanoparticles across an Imprinted Groove. *J. Appl. Crystallogr.* **2015**, *48*, 1827−1833.
(53) Korkmaz, S.; Kariper, A. Production and Applications of Flexible/Wearable Triboelectric Nanogenerator (TENGS). *Synth. Met.* **2021**, *273*, No. 116692.
(54) Xia, X.; Liu, Q.; Zhu, Y.; Zi, Y. Recent Advances of Triboelectric Nanogenerator Based Applications in Biomedical Systems. *EcoMat* **2020**, *2*, No. e12049.
(55) Kim, D. W.; Lee, J. H.; Kim, J. K.; Jeong, U. Material Aspects of Triboelectric Energy Generation and Sensors. *NPG Asia Mater.* **2020**, *12*, No. 6.
(56) Park, S.; Seol, M.; Jeon, S.; Kim, D.; Lee, D.; Choi, K. Surface Engineering of Triboelectric Nanogenerator with an Electrodeposited Gold Nanoflower Structure. *Sci. Rep.* **2015**, *5*, No. 13866.
(57) Wu, W.; Zhang, X.; Qin, L.; Li, X.; Meng, Q.; Shen, C.; Zhang, G. Enhanced MPBR with Polyvinylpyrrolidone-Graphene Oxide/PVDF Hollow Fiber Membrane for Efficient Ammonia Nitrogen Wastewater Treatment and High-Density Chlorella Cultivation. *Chem. Eng. J.* **2020**, *379*, No. 122368.
(58) Lanceros-Méndez, S.; Mano, J. F.; Costa, A. M.; Schmidt, V. H. FTIR and DSC Studies of Mechanically Deformed β-PVDF Films. *J. Macromol. Sci., Part B* **2001**, *40*, 517−527.
(59) Yang, W.; Li, Y.; Feng, L.; Hou, Y.; Wang, S.; Yang, B.; Hu, X.; Zhang, W.; Ramakrishna, S. GO/Bi2S3 Doped PVDF/TPU Nanofiber Membrane with Enhanced Photothermal Performance. *Int. J. Mol. Sci.* **2020**, *21*, No. 4224.
(60) Asefnejad, A.; Khorasani, M. T.; Behnamghader, A.; Farsadzadeh, B.; Bonakdar, S. Manufacturing of Biodegradable Polyurethane Scaffolds Based on Polycaprolactone Using a Phase Separation Method: Physical Properties and in Vitro Assay. *Int. J. Nanomed.* **2011**, *6*, 2375−2384.
(61) Fallahiarezoudar, E.; Ahmadipourroudposht, M.; Idris, A.; Yusof, N. M. Optimization and Development of Maghemite (γ-Fe2O3) Filled Poly-L-Lactic Acid (PLLA)/Thermoplastic Polyurethane (TPU) Electrospun Nanofibers Using Taguchi Orthogonal Array for Tissue Engineering Heart Valve. *Mater. Sci. Eng. C* **2017**, *76*, 616−627.
(62) Li, J. W.; Lee, H. T.; Tsai, H. A.; Suen, M. C.; Chiu, C. W. Synthesis and Properties of Novel Polyurethanes Containing Long-Segment Fluorinated Chain Extenders. *Polymers* **2018**, *10*, No. 1292.
(63) Canet-Ferrer, J.; Coronado, E.; Forment-Aliaga, A.; Pinilla-Cienfuegos, E. Correction of the Tip Convolution Effects in the Imaging of Nanostructures Studied through Scanning Force Microscopy. *Nanotechnology* **2014**, *25*, No. 395703.
(64) Zhu, G.; Bai, P.; Chen, J.; Lin Wang, Z. Power-Generating Shoe Insole Based on Triboelectric Nanogenerators for Self-Powered Consumer Electronics. *Nano Energy* **2013**, *2*, 688−692.
(65) Pu, X.; Zha, J. W.; Zhao, C. L.; Gong, S. B.; Gao, J. F.; Li, R. K. Y. Flexible PVDF/Nylon-11 Electrospun Fibrous Membranes with Aligned ZnO Nanowires as Potential Triboelectric Nanogenerators. *Chem. Eng. J.* **2020**, *398*, No. 125526.
(66) Jing, Q.; Kar-Narayan, S. Nanostructured Polymer-Based Piezoelectric and Triboelectric Materials and Devices for Energy Harvesting Applications. *J. Phys. D: Appl. Phys.* **2018**, *51*, No. 303001.
(67) Dzhardimalieva, G. I.; Yadav, B. C.; Lifintseva, T. V.; Uflyand, I. E. Polymer Chemistry Underpinning Materials for Triboelectric Nanogenerators (TENGs): Recent Trends. *Eur. Polym. J.* **2021**, *142*, No. 110163.
(68) Chowdhury, A. R.; Abdullah, A. M.; Hussain, I.; Lopez, J.; Cantu, D.; Gupta, S. K.; Mao, Y.; Danti, S.; Uddin, M. J. Lithium Doped Zinc Oxide Based Flexible Piezoelectric-Triboelectric Hybrid Nanogenerator. *Nano Energy* **2019**, *61*, 327−336.
(69) Abdullah, A. M.; Flores, A.; Chowdhury, A. R.; Li, J.; Mao, Y.; Uddin, M. J. Synthesis and Fabrication of Self-Sustainable Triboelectric Energy Case for Powering Smart Electronic Devices. *Nano Energy* **2020**, *73*, No. 104774.
(70) Pu, X.; Liu, M.; Chen, X.; Sun, J.; Du, C.; Zhang, Y.; Zhai, J.; Hu, W.; Wang, Z. L. Ultrastretchable, Transparent Triboelectric Nanogenerator as Electronic Skin for Biomechanical Energy Harvesting and Tactile Sensing. *Sci. Adv.* **2017**, *3*, No. 1700015.

https://doi.org/10.1021/acsami.1c17964
ACS Appl. Mater. Interfaces 2021, 13, 60401−60412